A strategy to suppress phonon transport in molecular junctions using π-stacked systems

Qian Li,[†] Mikkel Strange,[†] Ivan Duchemin,[‡] Davide Donadio,[§] and Gemma C. Solomon[*,†]

Nano-Science Center and Department of Chemistry, University of Copenhagen, DK-2100 Copenhagen Ø, Denmark., Univ Grenoble Alpes, F-38000 Grenoble, France, CEA, INAC SP2M/L_Sim, F-38054 Grenoble, France, and Department of Chemistry, University of California Davis, One Shields Avenue, Davis, CA, 95616.

E-mail: gsolomon@nano.ku.dk

Abstract

Molecular junctions are promising candidates for thermoelectric devices due to the potential to tune the electronic and thermal transport properties. However, a high figure of merit is hard to achieve, without reducing the phononic thermal conductance. Here, we propose a strategy to suppress phonon transport in graphene based molecular junctions preserving high electronic power factor using non-bonded π-stacked systems. From our calculations, we find that the thermal conductance of π-stacked systems can be reduced by about 95%, compared with that of a covalently bonded molecular junction. Phonon transmission of π-stacked systems is largely attenuated in the whole frequency range and the remaining transmission is

[*]To whom correspondence should be addressed

[†]Nano-Science Center and Department of Chemistry, University of Copenhagen, DK-2100 Copenhagen Ø, Denmark.

[‡]Univ Grenoble Alpes, F-38000 Grenoble, France

[¶]CEA, INAC SP2M/L_Sim, F-38054 Grenoble, France

[§]Department of Chemistry, University of California Davis, One Shields Avenue, Davis, CA, 95616.

mainly below 5 THz, where out-of-plane channels dominate. We find that the figure of merit ZT for the π-stacked molecular junction can be dramatically enhanced because of the very low phononic thermal conductance, without optimization of its electronic properties.

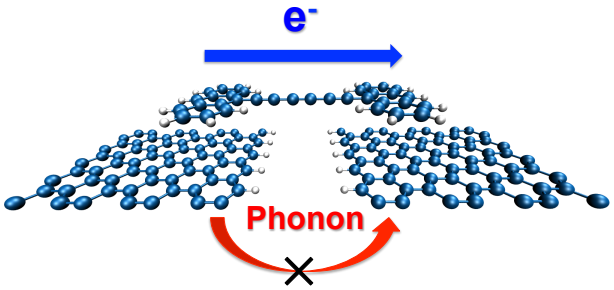

Table of contents graphic

Thermoelectric devices can directly convert temperature differences to an electric voltage, and vice versa. The efficiency of a thermoelectric device is characterized by the dimensionless figure of merit $ZT = S^2GT/\kappa$. Here S is the thermopower(or Seebeck coefficient), G is the electronic conductance, T is temperature and $\kappa = \kappa_e + \kappa_{ph}$ is the total thermal conductance with contributions from both electrons and phonons. In order to achieve a high value of ZT, one should maximize the power factor S^2G and minimize the thermal conductance κ. Molecular junctions are promising candidates for thermoelectric devices.[1] It has been shown that sharp transmission resonances near the Fermi energy achieved by tuning the chemical properties of the molecule and molecule-electrode contact can substantially enhance the thermopower.[2] Several works have investigated thermoelectric effects in molecular junctions using density functional theory (DFT) combined with Green's function method.[3–7] Saha et al. propose thermoelectric devices where a single molecule is connected to two metallic zigzag graphene nanoribbons.[4] Their results show that the figure of merit (ZT) is still low because of the large phononic thermal conductance κ_{ph}, although the junction's power factor is already optimized. Recently Bürkle et al. presented a theoretical study of the thermoelectric properties of [2,2]paracyclophane-based single-molecule junctions.[6] They emphasized that the high phononic contribution to the thermal conductance strongly suppresses ZT and it is necessary to include the phononic thermal conductanceκ_{ph} for molecular junctions in order

to obtain accurate and reliable predictions of ZT. Thus, understanding and suppressing phonon transport in molecular junctions is important for improving thermoelectric efficiency.

Sadeghi et al. showed a way to suppress phonon transmission by using a molecule that better transmits higher-frequency phonon modes, combined with a low-Debye-frequency electrode that filters high-energy phonons.[7] In addition, π-stacked systems, whose electronic coupling is through-space, are anticipated to have a low thermal conductance and thereby make them good candidates to achieve high thermoelectric figure of merit (ZT) in molecular junctions.[21] This π-π stacking structure was also studied in organic molecular crystals, with the phonon thermal conductivity calculated using classical molecular dynamics (MD) simulations.[22] In our previous work,[21] we investigated heat transport through π-stacked molecules connected with gold electrodes using a model system with parameters representing the force constants obtained from DFT. As the overlap of frequencies between gold and molecule is very narrow, only the centre-of-mass modes of the molecule were considered. We showed that thermal conductance can be either increased or decreased for a non-bonded π-stacked system, compared with an analogous single-molecule junction. It is worth investigating the effect of leads with a broader range of frequencies, that better match the modes of molecules. It is also highly desirable to study phonon transport through π-stacked molecular junctions including all phonon modes of the system using DFT.

Several remarkable experiments have been performed to measure the thermal conductance across heterointerfaces between solids and monolayers of organic molecules, and of heat dissipation in molecular junctions.[8–11] Losego et al. investigated the effect of chemical bonding on interfacial heat transport in Au|self-assembled monolayers|Quartz junctions.[10] They found that the interface thermal conductance was enhanced with a stronger (covalent) bond to the Au surface, compared with weaker (van der Waals) interactions. Meier et al. reported the length dependence of thermal transport across self-assembled monolayers of alkane chains using scanning thermal microscopy.[12] These experimental developments call for theoretical efforts to further understand and engineer heat transport in molecular junctions.

Recent experiments have proven that stable and gateable molecular junctions can be formed

by depositing molecules on top of a graphene nanogap fabricated by electroburning.[13–15] Replacing noble metals as the electrode with graphene has several advantages:[13,16] 1. Graphene has an excellent stability at high temperatures. 2. Compared with metallic electrodes, graphene allows for a large variety of possibilities to anchor diverse molecules. 3. In the carbon-based junctions, individual molecules can bind to the graphene leads not only covalently [17] but also via π-π stacking of aromatic rings. 4. Graphene leads can enhance electrostatic gating as a result of the reduced screening. Several theoretical works have addressed the electronic properties of graphene-molecule-graphene junctions.[16,18–20] However, a comprehensive thermoelectric characterization of such molecular junctions with anchor groups coupling to the graphene leads through π-π stacking, in which electron and phonon transport are treated on equal footing by first principles is still lacking.

In this paper, we propose the use of π-π stacking as a promising strategy to realize thermoelectric molecular junctions with high figure of merit, as π-stacked systems retain high power factor while their thermal conductance is largely suppressed. We employ first-principles DFT to relax the structures and to compute the force constants matrix. Then the thermal conductance of the molecular junction is calculated considering all modes of the system using the elastic scattering matrix approach.[23] The specific contributions of phonons with different polarization to phonon transport are also analyzed. We then compute the electronic transport coefficients of two representative molecular junctions at DFT level using non-equilibrium Green's functions. It is found that reducing phononic thermal conductance can significantly improve the figure of merit in these all-carbon molecular junctions.

Here we investigate four systems: (a) C1, (b) CC11, (c) CC13, (d) PA, as shown in the left panel of Figure 1. C1 represents a single-molecule junction, while CC11, CC13 are non-bonded π-stacked systems. Note that CC13 has mass-mismatch in the molecules. The molecules' chemical structures are shown correspondingly in the right panel in Figure 1. The molecules were covalently bonded with the graphene leads with terminal hydrogen atoms removed. Recent experiments[13–15] also suggest a more realistic way to use π-π stacking in the molecular junction with graphene leads,

where the molecules' anchor groups bind to the surface of graphene through π-π interactions. PA is the experiment relevant structure we investigated here. PA consists of two anthracenes as anchor groups coupling with graphene leads through π-π interaction and a six-carbon (C6) alkyne chain as a central molecule, shown in Figure 1(d). The molecule is adsorbed on the surface of the graphene layer with AB stacking, which is the most stable structure.[16,24,25]

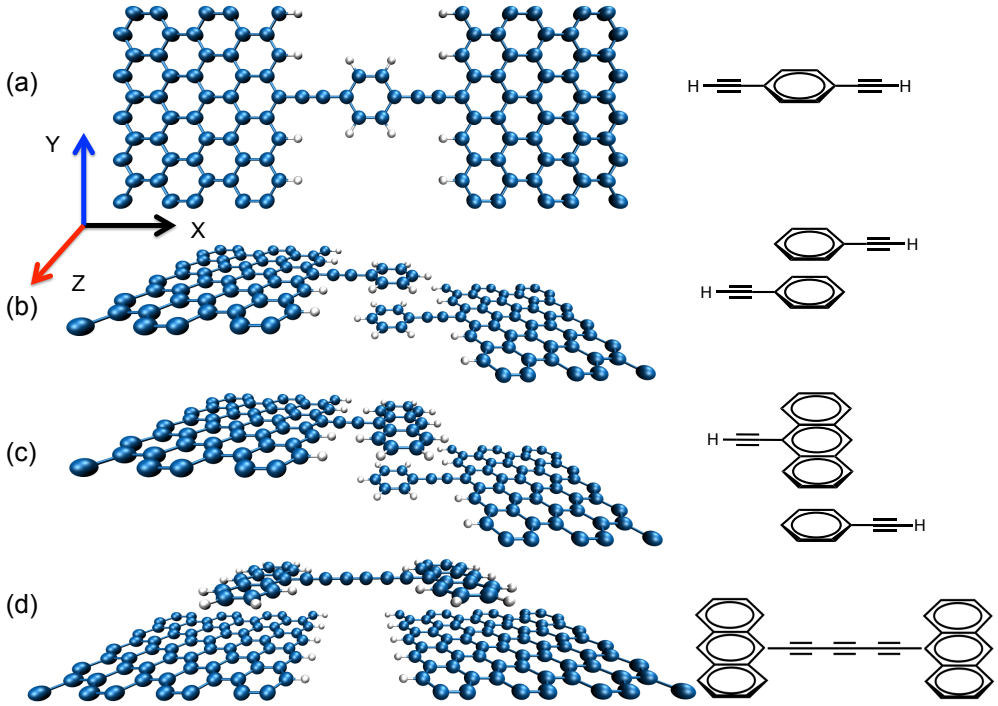

Figure 1: (a) A molecular junction with a single molecule(C1). (b) A molecular junction with π-stacked molecules(CC11). (c) A molecular junction with mass-mismatch π-stacked molecules(CC13). (d) Anthracenes are used as anchor groups coupling with graphene leads through π-π stacking and the central molecule is a six-carbon alkyne chain (PA). The right panel shows the chemical structure of each molecule in the junction correspondingly.

In the elastic phonon scattering calculation, the molecular junction is divided into three parts: the central region and two semi-infinite leads acting as thermal baths at different temperature.[26] The molecular junction is oriented so that heat current flows along the x axis. The central region includes the molecule and a part of the graphene leads, which are saturated with hydrogen atoms. The graphene lead has 2-3 principal layers, where each principal layer includes 40 carbon atoms. Geometry optimizations and the calculation of force constants matrices are performed using Quan-

tum Espresso.[27] We use the local density approximation (LDA)[28] and treat core electrons using ultrasoft pseudopotentials.[29] Prior theoretical results have demonstrated that LDA provides a reasonably accurate description of the binding between achromatic rings and graphene or interlayer of graphene.[30–32] The stacking distance we obtained is ~ 3.35 Å, which is in agreement with the previous values. The Kohn-Sham wave functions and the charge density are expanded in plane waves up to energy cutoffs of 35 Ry and 300 Ry, respectively. We set Methfessel-Paxton smearing [33] with an energy width of 0.02 Ry. Periodic boundary conditions are applied in the calculations, so the graphene leads are infinite. Periodic replicas of the system in the z direction are separated by a vacuum region of 13.5 Å, which is sufficient to make the interactions between layers negligible. A $4\times4\times1$ k-point mesh for the graphene leads and a $1\times4\times1$ k-point mesh for the central region are used in the calculation of the force constants.

Phonon transmission is calculated using lattice dynamics and the elastic scattering kernel method.[34] Since anharmonic scattering has limited impact on phonon transport in short all-carbon molecular junctions,[35,36] we only consider harmonic approximation here. In harmonic lattice dynamics the phononic properties are fully determined by the force constant matrix, K, which is calculated by finite differences:

$$K_{i\alpha,j\beta} = \frac{\partial^2 E}{\partial \mu_{i\alpha} \partial \mu_{j\beta}} = -\frac{F_{j\beta}(Q_{i\alpha}) - F_{j\beta}(-Q_{i\alpha})}{2Q_{i\alpha}} \tag{1}$$

where $\mu_{i\alpha}(\mu_{j\beta})$ is the displacement of atom $i(j)$ in the $\alpha(\beta)$ coordinate direction and E is the total energy.[26] The central region of the molecular junction is initially relaxed to a maximum residual force of 0.001 Ry/Bohr. Then each atom i, is displaced by $Q_{i\alpha} = \pm 0.02$ Å in the direction $\alpha = x, y, z$ to obtain the forces $F_{j\beta}(Q_{i\alpha})$, on atom j along the β coordinate. The dynamical matrix D can be obtained from the force constant matrix $D_{i\alpha,j\beta} = K_{i\alpha,j\beta}/\sqrt{m_i m_j}$, where $m_i(m_j)$ is the mass of atom $i(j)$. Then the dynamical matrices of the device and of the graphene leads are used to calculate the elastic scattering matrix [23] using the kernel method described in Ref.[34] Assuming the temperature difference tends to zero, the phonon transmission function between the two thermal baths A and B

is expressed as:

$$\tau_{AB}(\omega) = \sum_{i\in A}\sum_{j\in B} |S_{ij}(\omega)|^2 \tag{2}$$

where the scattering tensor $S(\omega)$ maps the incoming phonons onto the outgoing phonons for each frequency ω. The corresponding phononic thermal conductance is given by the Laudauer formula:

$$\kappa_{AB}(T) = \int_0^\infty \frac{\hbar\omega}{2\pi}\tau_{AB}(\omega)\frac{\partial f(\omega,T)}{\partial T}d\omega \tag{3}$$

where $f(\omega,T) = 1/[\exp(\hbar\omega/k_BT) - 1]$ is the Bose-Einstein distribution function at the temperature T of the lead.

The electronic transport calculations have been performed with a Green's function implementation of the Landauer-Büttiker approach:

$$I(V) = \frac{2e}{h}\int_{-\infty}^{\infty} \mathrm{d}E(f_\mathrm{L} - f_\mathrm{R})\mathscr{T}_\mathrm{e}(E), \tag{4}$$

where $f = 1/\{\exp[(E-\mu_\alpha)/(k_\mathrm{B}T)] + 1\}$ is the Fermi-Dirac distribution function for the leads $\alpha = \mathrm{L},\mathrm{R}$ with the chemical potential μ_α and $\mathscr{T}_\mathrm{e}(E)$ is the electronic transmission. Following the standard DFT-Landauer approach, the zero-bias electron transmission function between left lead and right lead is expressed as

$$\mathscr{T}_\mathrm{e}(E) = \mathrm{Tr}[\Gamma_\mathrm{L}G^R\Gamma_\mathrm{R}G^A], \tag{5}$$

where Γ_L and Γ_R are half the imaginary parts of the left and right electrode self-energies, respectively, and G^R and G^A are the retarded and advanced Green's functions of the scattering region. The electronic transmissions are calculated with the GPAW[37] code using an atomic orbital basis set corresponding to double-zeta plus polarization and the Perdew-Burke-Ernzerhof (PBE) exchange-correlation functional. The Monckhorst-Pack k-point sampling is taken in the transverse direction of graphene leads, since the transmission exhibits a strong k-point dependence.[38,39] The electronic transmission is obtained from averaging over $1 \times 128 \times 1$ k points. When inelastic scattering is

neglected, the transport coefficients relevant for thermoelectricity can be expressed as

$$G = e^2 L_0, \quad S = \frac{1}{eT}\frac{L_1}{L_0}, \quad \kappa_{\mathrm{e}} = \frac{1}{T}\left(L_2 - \frac{L_1^2}{L_0}\right), \tag{6}$$

in terms of the function

$$L_n = \frac{2}{h}\int_{-\infty}^{+\infty} \mathrm{d}E (E-\mu)^n \left(-\frac{\partial f(E,\mu,T)}{\partial E}\right) \mathscr{T}_{\mathrm{e}}(E). \tag{7}$$

The dimensionless figure of merit can be given by $ZT = S^2 GT/(\kappa_e + \kappa_{ph})$.

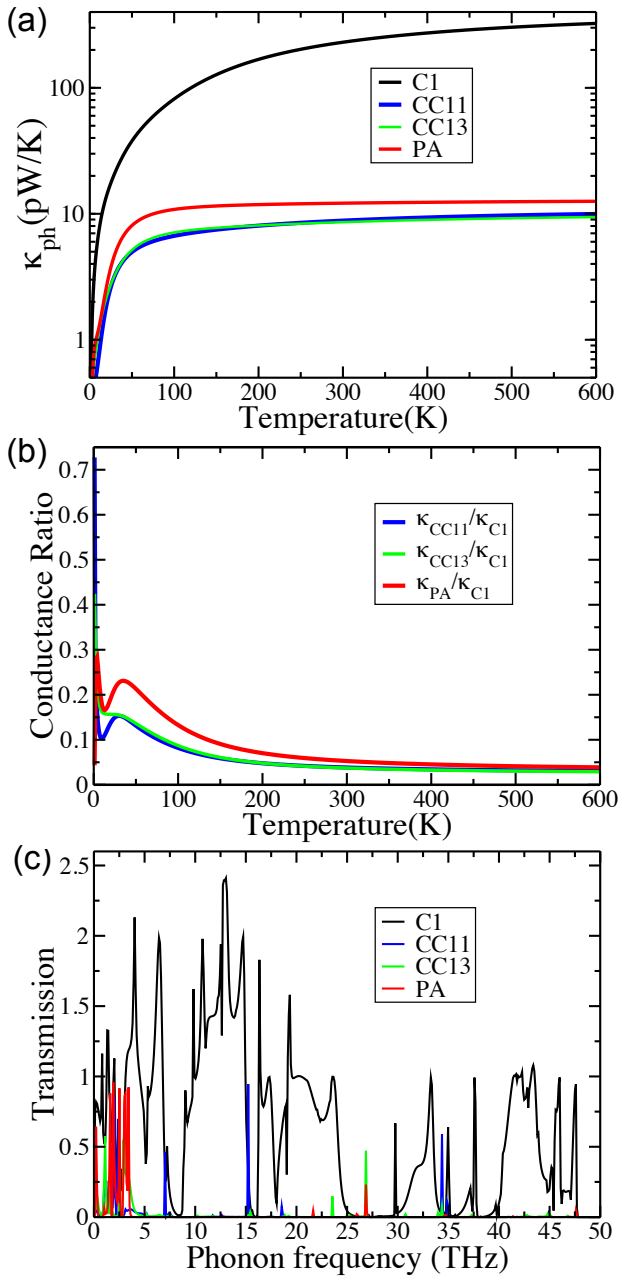

Figure 2: (a) Phononic thermal conductance κ_{ph} (on a log scale) as a function of temperature for these four molecular junctions: C1, CC11, CC13 and PA. (b)The phononic conductance ratio of $\kappa_{CC11}/\kappa_{C1}$, $\kappa_{CC13}/\kappa_{C1}$ and κ_{PA}/κ_{C1}. (c) Phonon transmission as a function of frequencies for C1, CC11, CC13 and PA.

The phononic thermal conductance and phonon transmission of molecular junctions C1, CC11, CC13 and PA are calculated and shown in Figure 2. The thermal conductance of the single molecular junction C1 is high and can reach 230 pW/K at 300K. Figure 2(a) shows that the thermal

conductance of CC11, CC13 and PA are significantly reduced, compared with that of C1. If we only compare three π-stacked systems, we can see that the thermal conductance of PA is slightly higher than CC11 and CC13. However, the thermal conductance of all theses π-stacked molecular junctions are generally low. CC11 is 8.8 pW/K, CC13 is 8.6 pW/K, and PA is 12 pW/K at 300 K. Although CC13 has mass mismatch in the molecules, the thermal conductance of CC13 is very similar to that of CC11. Unlike what we saw previously for π-stacked molecules bonded to Au electrodes,[21] the mass mismatch effect does not seem to play an important role here. The thermal conductance ratio defined as $\kappa_{CC11}/\kappa_{C1}$, $\kappa_{CC13}/\kappa_{C1}$ and κ_{PA}/κ_{C1}, is also plotted and shown in Figure 2(b). At very low temperature the conductance ratios are the largest, meaning that the lowest frequency acoustic modes can still be transported by π-stacked structures. Then the ratios decrease dramatically with temperature. The conductance ratios of CC11 and CC13 are both 4% and PA is 5% at 300 K. These results show that phonon transport can be blocked significantly in these π-stacked systems, compared with the fully covalent single-molecule junction C1. Figure 2(c) shows that there are intense and broad peaks below 25 THz in the phonon transmission of C1, which result in the high thermal conductance of C1. In contrast, the phonon transmission of CC11, CC13 and PA are dramatically attanuated in the whole frequency range. The residual transmission through CC11, CC13 and PA is mainly below 5 THz and there are only several discrete sharp peaks in the frequency range between 5 THz and 50 THz. So the thermal conductance for π-stacked systems is mainly contributed by frequencies below 5 THz.

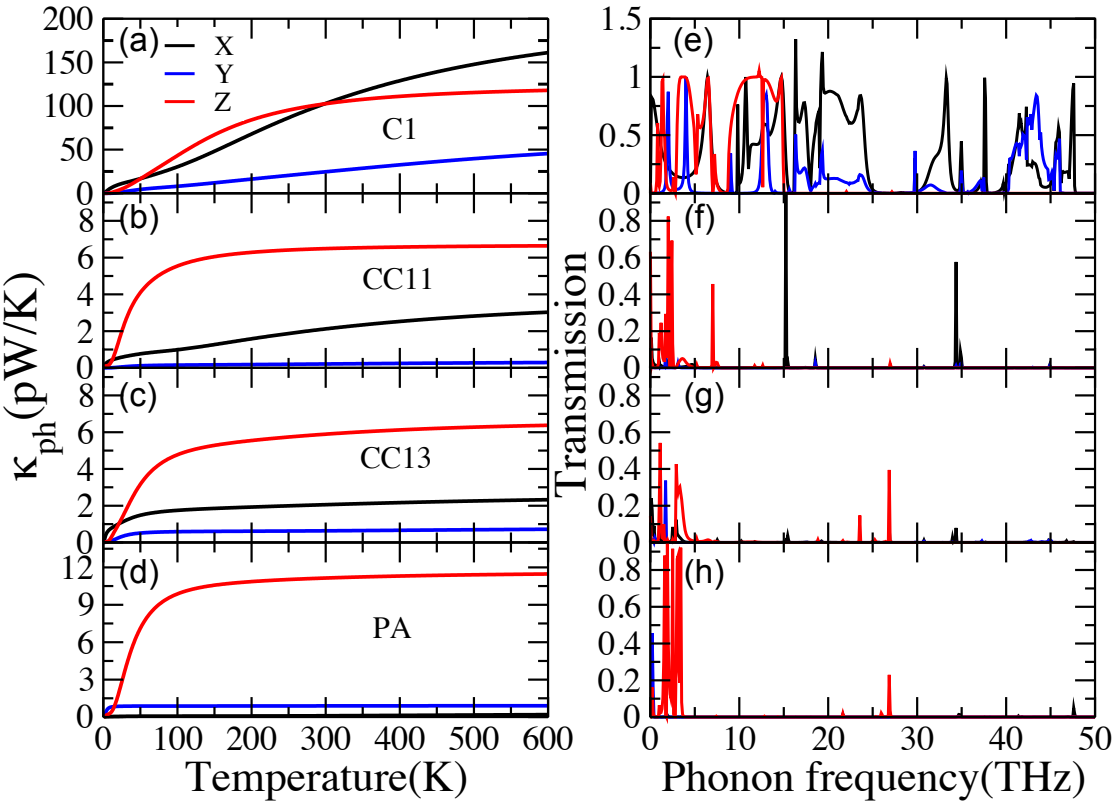

Figure 3: Phononic thermal conductance and phonon transmission selected according to the polarization of the incoming phonon channels of the graphene leads, for C1(the first panel), CC11(the second panel), CC13(the third panel) and PA(the fourth panel). X, Y and Z components correspond to longitudinal, in-plane transverse and out of plane modes.

To gain further insight into the transmission spectrum, we also study the phonon conductance and transmission by polarization of the incoming channels. Figure 3 shows the conductance and transmission contributions from x (longitudinal mode), y (in-plane transverse mode), and z (out-of-plane flexural mode) channels for C1, CC11, CC13 and PA. The phonon conductance by polarization of C1 shows that the x and z channels provide a larger contribution than the y channel (Figure 3(a)). This behaviour is similar to thermal transport in pristine graphene, where the flexural modes play an important role.[40] Figure 3(b, c and d) shows that the phonon conductance of all channels in CC11, CC13 and PA are significantly suppressed. For CC11 and CC13, there are still some contributions from the x channel. In the case of PA, the thermal conductance from in-plane modes is close to zero. We can see that the z channel dominates in all these π-stacked systems. These results can be interpreted by considering the chemical structure of the systems. π-π stacking

results in appreciable mechanical coupling in the z direction, holding the system together, while there is relatively weak interaction in the x and y directions. Thus, out-of-plane modes with the strongest coupling transport most of the heat in these π-stacked molecular junctions.

Phonon transmission by polarization of C1 (Figure 3(e)) shows that transmission from the z channel provides the largest contribution below 15 THz, followed by x channel, leading to a relatively high thermal conductance. By contrast, for the π-stacked systems, z channel dominates below 5 THz, shown in Figure 3(f,g and h). Above 5 THz, very few peaks are observed for any polarization. These results show that heat transport in π-stacked system is limited to out-of-plane center of mass modes. Further reduction of the phononic thermal conductance should therefore focus on reducing the contribution of out-of-plane modes to the thermal conductance of the π-stacked systems.

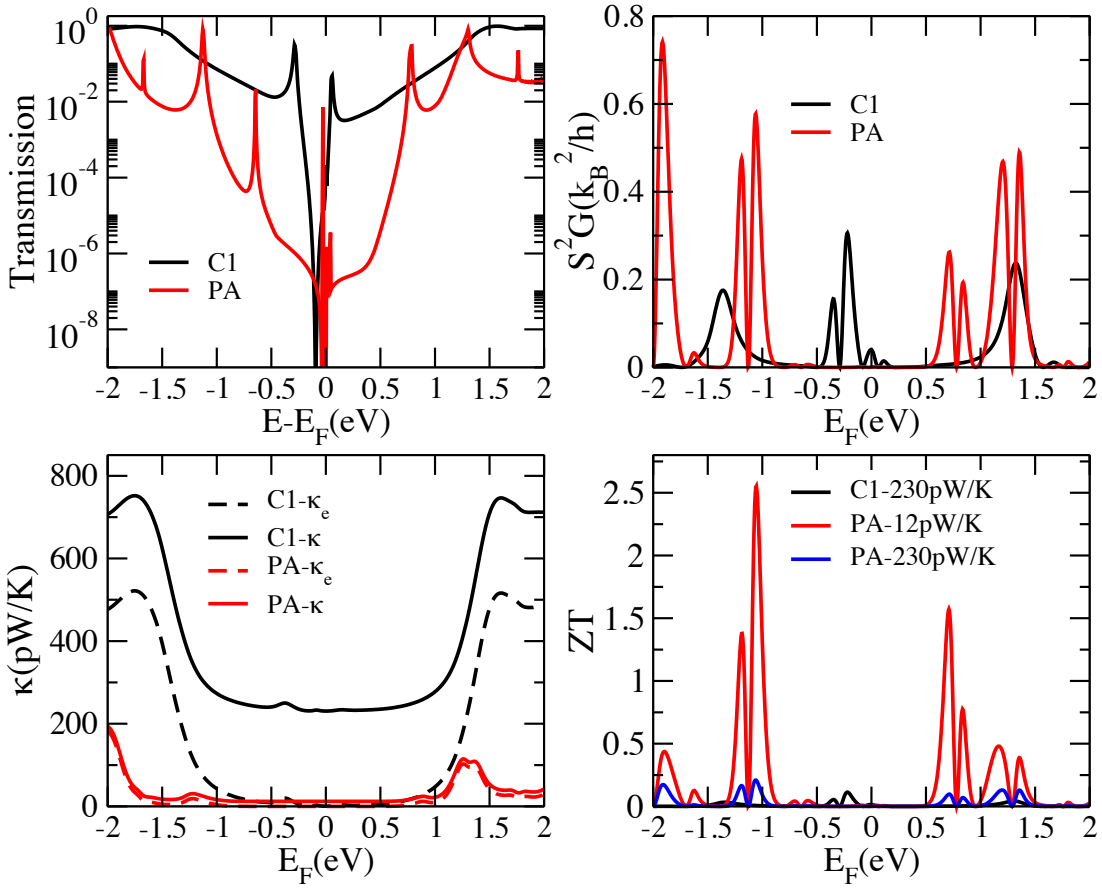

Figure 4: (a) Electronic transmission for C1 and PA. (b) Power factor S^2G as a function of energy for C1 and PA. (c) Electronic thermal conductance (dashed line) and total thermal conductance (solid line) for C1 and PA. (d) Thermoelectric figure of merit ZT as a function of energy for C1 and PA with different phononic thermal conductance.

In order to investigate how the reduction of phononic thermal conductance influences the thermoelectric efficiency of molecular junctions, we calculated the electronic and thermoelectric properties of two representative molecular junctions, C1 and PA, as described in the methods section. Since the thermoelectric properties depend on the Fermi energy of the leads and could be tuned by electrostatic or electrochemical gating or doping, we calculated the power factor, electronic thermal conductance and total thermoelectric figure of merit as a function of electrochemical potential, shown in Figure 4.

Figure 4(a) shows that the electronic transmission near the Fermi energy for both PA and C1 is very low, which originates from the band structure of the graphene leads and from the electronic

coupling between the molecule and graphene layer.[16] It can be seen that the low transmission region near the Fermi energy of C1 is much narrower than that of PA, and the electronic conductance of C1 is generally higher. The maximal power factor S^2G for C1 near the Fermi energy is about 0.3 k_B^2/h at -0.22 eV. For PA, power factor near the Fermi energy is very low, while there are a maximum of 0.577 k_B^2/h at -1.0 eV and a local maximum of 0.26 k_B^2/h at 0.71 eV (Figure 4(b)). Figure 4(c) shows that the electronic thermal conductance of both C1 and PA near the Fermi energy is very low and close to each other. The total thermal conductance of PA does not change much due to the very small contribution from phonons (12 pW/K). However, the total thermal conductance of C1 increases a lot and is much higher than PA, because of the high value of the phononic thermal conductance (230 pW/K). As a result, the figure of merit ZT of C1 is generally very low and the maximum is only 0.113 at -0.22 eV(Figure 4(d)), although C1 has a high electronic conductance, good power factor and low electronic thermal conductance near the Fermi energy. In contrast, the figure of merit of PA can reach a maximum of 2.55 at -1.0 eV(p-doping) and a local maximum of 1.57 at 0.71 eV(n-doping) at 300 K, because of the very low phononic thermal conductance(12 pW/K), shown in Figure 4(d) . To highlight the importance of the suppression of thermal conductance in π-stacked systems, we calculated the figure of merit of PA assuming a phononic thermal conductance 230 pW/K, like that C1. It can be seen that the figure of merit of PA gets dramatically suppressed, in the same range as that computed for C1. These calculations prove that also in molecular junctions it is crucial to suppress the phononic thermal conductance to significantly improve the thermoelectric figure of merit. It is remarkable that it can be achieved without introducing new chemical elements in the systems, but just exploiting the chemical versatility of carbon.

In conclusion, we found that the phononic thermal conductance of non-bonded π-stacked systems can be reduced by 95%, compared with that of a covalently bonded molecular junction C1. The phonon transmission of CC11, CC13 and PA is dramatically attenuated in the whole frequency range and the residual transmission is mainly from center-of-mass modes below 5 THz. The phonon conductance from all channels in π-stacked systems are significantly reduced. However, z channel dominates in the residual transmission, due to the strong coupling along the z

direction in π-π stacking. Comparing the thermoelectric figure of merit of the C1 and the PA junctions, we showed that suppressing heat transport in molecular junction by π-π stacking can be exploited to optimize their thermoelectric performance. Although C1 has a high electron conductance, good power factor, low electronic thermal conductance near Fermi energy, the ZT of C1 is very low due to the large contribution of phonons. By contrast, the ZT of PA can reach 2.55 at -1.0 eV at 300 K because of its very low phononic thermal conductance.

The molecular junctions considered in this work are a showcase to demonstrate the importance of phononic thermal conductance, but they are not optimal for thermoelectric energy conversion. One can envisage that gating [4,13,41,42] or doping [16,43,44] the graphene leads combined with appropriate modifications to the bridging molecules could lead to very favourable thermoelectric characters. Since the phononic thermal conductance has been dramatically reduced in these π-stacked systems and is largely independent of electronic properties, it leaves an open question for future work to tune electronic properties of these molecular junctions to achieve high ZT in closer proximity to the Fermi level.

Acknowledgement

We thank Anders Borges for the help with the electron transport calculations. This work was supported by the funding from the European Research Council under the European Union's Seventh Framework Program (FP7/2007- 2013)/ERC Grant Agreement No. 258806 and The Danish Council for Independent Research Natural Sciences. Calculations have been performed at the Rechenzentrum Garching of the Max Planck Society.

References

(1) Reddy, P.; Jang, S.-Y.; Segalman, R. A.; Majumdar, A. *Science* **2007**, *315*, 1568–1571.

(2) Bergfield, J. P.; Stafford, C. A. *Nano Lett.* **2009**, *9*, 3072–3076.

(3) Nozaki, D.; Sevinçli, H.; Li, W.; Gutiérrez, R.; Cuniberti, G. *Phys. Rev. B* **2010**, *81*, 235406.

(4) Saha, K. K.; Markussen, T.; Thygesen, K. S.; Nikolić, B. K. *Phys. Rev. B* **2011**, *84*, 041412.

(5) Nikolić, B. K.; Saha, K. K.; Markussen, T.; Thygesen, K. S. *J. Comput. Electron.* **2012**, *11*, 78–92.

(6) Bürkle, M.; Hellmuth, T. J.; Pauly, F.; Asai, Y. *Phys. Rev. B* **2015**, *91*, 165419.

(7) Sadeghi, H.; Sangtarash, S.; Lambert, C. J. *Nano Lett.* **2015**, *15*, 7467–7472.

(8) Lee, W.; Kim, K.; Jeong, W.; Zotti, L. A.; Pauly, F.; Cuevas, J. C.; Reddy, P. *Nature* **2013**, *498*, 209–212.

(9) Wang, Z.; Carter, J. A.; Lagutchev, A.; Koh, Y. K.; Seong, N.-H.; Cahill, D. G.; Dlott, D. D. *Science* **2007**, *317*, 787–790.

(10) Losego, M. D.; Grady, M. E.; Sottos, N. R.; Cahill, D. G.; Braun, P. V. *Nat. Mater.* **2012**, *11*, 502–506.

(11) Majumdar, S.; Sierra-Suarez, J. A.; Schiffres, S. N.; Ong, W.-L.; Higgs, C. F.; McGaughey, A. J. H.; Malen, J. A. *Nano Lett.* **2015**, *15*, 2985–2991.

(12) Meier, T.; Menges, F.; Nirmalraj, P.; Hölscher, H.; Riel, H.; Gotsmann, B. *Phys. Rev. Lett.* **2014**, *113*, 060801.

(13) Prins, F.; Barreiro, A.; Ruitenberg, J. W.; Seldenthuis, J. S.; Aliaga-Alcalde, N.; Vandersypen, L. M.; van der Zant, H. S. *Nano Lett.* **2011**, *11*, 4607–4611.

(14) Ullmann, K.; Coto, P. B.; Leitherer, S.; Molina Ontoria, A.; Martín, N.; Thoss, M.; Weber, H. B. *Nano Lett.* **2015**, *15*, 3512–3518.

(15) Lau, C. S.; Sadeghi, H.; Rogers, G.; Sangtarash, S.; Dallas, P.; Porfyrakis, K.; Warner, J.; Lambert, C. J.; Briggs, G. A. D.; Mol, J. A. *Nano Lett.* **2015**, *16*, 170–176.

(16) Li, Y.; Tu, X.; Wang, H.; Sanvito, S.; Hou, S. *J. Chem. Phys.* **2015**, *142*, 164701.

(17) Guo, X. et al. *Science* **2006**, *311*, 356–359.

(18) Péterfalvi, C. G.; Lambert, C. J. *Phys. Rev. B* **2012**, *86*, 085443.

(19) García-Suárez, V. M.; Ferradás, R.; Carrascal, D.; Ferrer, J. *Phys. Rev. B* **2013**, *87*, 235425.

(20) Sadeghi, H.; Sangtarash, S.; Lambert, C. J. *Beilstein J. Nanotechnol.* **2015**, *6*, 1413–1420.

(21) Kiršanskas, G.; Li, Q.; Flensberg, K.; Solomon, G. C.; Leijnse, M. *Appl. Phys. Lett.* **2014**, *105*, 233102.

(22) Mi, X.-Y.; Yu, X.; Yao, K.-L.; Huang, X.; Yang, N.; Lü, J.-T. *Nano Lett.* **2015**, *15*, 5229–5234.

(23) Young, D. A.; Maris, H. J. *Phys. Rev. B* **1989**, *40*, 3685.

(24) Björk, J.; Hanke, F.; Palma, C.-A.; Samori, P.; Cecchini, M.; Persson, M. *J. Phys. Chem. Lett.* **2010**, *1*, 3407–3412.

(25) Wang, W.; Zhang, Y.; Wang, Y.-B. *J. Chem. Phys.* **2014**, *140*, 094302.

(26) Li, Q.; Duchemin, I.; Xiong, S.; Solomon, G. C.; Donadio, D. *J. Phys. Chem. C* **2015**, *119*, 24636–24642.

(27) Giannozzi, P. et al. *J. Phys.: Condens. Matter* **2009**, *21*, 395502.

(28) Perdew, J. P.; Zunger, A. *Phys. Rev. B* **1981**, *23*, 5048–5079.

(29) Vanderbilt, D. *Phys. Rev. B* **1990**, *41*, 7892–7895.

(30) Yan, J.-A.; Ruan, W.; Chou, M. *Phys. Rev. B* **2008**, *77*, 125401.

(31) Kong, B. D.; Paul, S.; Nardelli, M. B.; Kim, K. W. *Phys. Rev. B* **2009**, *80*, 033406.

(32) Su, Y. H.; Wu, Y. K.; Tu, S.-L.; Chang, S.-J. *Appl. Phys. Lett.* **2011**, *99*, 163102.

(33) Methfessel, M.; Paxton, A. T. *Phys. Rev. B* **1989**, *40*, 3616–3621.

(34) Duchemin, I.; Donadio, D. *Phys. Rev. B* **2011**, *84*, 115423.

(35) Segal, D.; Nitzan, A.; Hänggi, P. *J. Chem. Phys.* **2003**, *119*, 6840–6855.

(36) Sasikumar, K.; Keblinski, P. *J. Appl. Phys.* **2011**, *109*, 114307.

(37) Enkovaara, J. et al. *J. Phys.: Condens. Matter* **2010**, *22*, 253202.

(38) Falkenberg, J. T.; Brandbyge, M. *Beilstein J. Nanotechnol.* **2015**, *6*, 1603–1608.

(39) Hüser, F.; Solomon, G. C. *J. Chem. Phys.* **2015**, *143*, 214302.

(40) Lindsay, L.; Broido, D. A.; Mingo, N. *Phys. Rev. B* **2010**, *82*, 115427.

(41) Oostinga, J. B.; Heersche, H. B.; Liu, X.; Morpurgo, A. F.; Vandersypen, L. M. *Nat. Mater* **2008**, *7*, 151–157.

(42) Papior, N.; Gunst, T.; Stradi, D.; Brandbyge, M. *Phys.Chem.Chem.Phys.* **2016**, *18*, 1025–1031.

(43) Lherbier, A.; Blase, X.; Niquet, Y.-M.; Triozon, F. m. c.; Roche, S. *Phys. Rev. Lett.* **2008**, *101*, 036808.

(44) Farmer, D. B.; Lin, Y.-M.; Afzali-Ardakani, A.; Avouris, P. *Appl. Phys. Lett.* **2009**, *94*, 213106.